Capillarity

Vol. 12, No. 1, p. 17-26, 2024

Original article

Visualizing oil displacement by nanofluids at pore scale: A concentration-dependent nanofluid spreading induced by structural disjoining pressure

Thakheru Akamine[1], Teerapat Tosuai[1], Romal Ramadhan[1], Natthanan Promsuk[2], Falan Srisuriyachai[3], Suparit Tangparitkul[1]*

[1]*Department of Mining and Petroleum Engineering, Faculty of Engineering, Chiang Mai University, Chiang Mai 50200, Thailand*
[2]*Department of Computer Engineering, Faculty of Engineering, Chiang Mai University, Chiang Mai 50200, Thailand*
[3]*Department of Mining and Petroleum Engineering, Faculty of Engineering, Chulalongkorn University, Bangkok 10330, Thailand*

Keywords:
Fluid displacement
flow in porous media
micromodel
nanoparticles
wettability alteration
capillary

Cited as:
Akamine, T., Tosuai, T., Ramadhan, R., Promsuk, N., Srisuriyachai, F., Tangparitkul, S. Visualizing oil displacement by nanofluids at pore scale: A concentration-dependent nanofluid spreading induced by structural disjoining pressure. Capillarity, 2024, 12(1): 17-26.
https://doi.org/10.46690/capi.2024.07.03

Abstract:
Immiscible fluid displacement in porous media is governed by pore-scale behaviors, which can be manipulated by chemical additives to engineer the process toward a greater turn-out. Although recent advances in nanofluids have been reported to influence such a process, their interfacial phenomena are likely controversial and need independent cross-examinations. As non-energetically interfacial responsive nanoparticles, silica cores adorned with polyvinylpyrrolidone were examined for their direct contribution to crude oil displacement performance at relatively low concentrations, ranging from 10 to 500 ppm, in the current study. The crude oil displacement was experimented via water-wet borosilicate micromodel and visualized to elucidate pore-scale interfacial phenomena involved. Concentration-dependent property of nanofluids was found, evidenced by different pore-scale mechanisms observed. At low concentrations (10 and 50 ppm), wetting layer flow controlled the oil displacement and led to swelling into pore space, inducing snap-off events and hence high oil ganglia trapped (> 300). At higher concentrations (100 ppm), nanoparticle self-arrangement at the water wedge was more effective, which induced oscillatory structural disjoining pressures between the oil-aqueous and solid-aqueous interfaces leading to narrow nanofluid spreading. Hence, the spatiotemporal displacement performed differently at high concentrations (displacement efficiencies were 36.8% at 100 ppm and 43.1% at 500 ppm), with snap-off hardly observed. At 500 ppm, more stable and stronger nanofilm spreading was developed due to meniscus expansion, obtaining faster-displacing dynamics (54.9% per pore volume injected) and additional oil displaced (+5.7%) after breakthrough time. The findings amplify nanofluid contribution and emphasize its concentration dependence on immiscible fluid flow in porous media, a potential applicability to various fields including enhanced oil recovery and CO_2 geological storage.

1. Introduction

One of multiphase flow processes that are relevant to a wide range of applications is an immiscible flow in porous media. Such a challenge covers everything from coffee filtering to larger flows in deep geological formations. The latter has been heavily researched in recent decades to address georesources security and tackle the climate crisis, namely petroleum production and CO_2 geological storage, respectively (Blunt, 2017). Given the same theoretical backgrounds to engineer the process, more complex flow improvement in

Yandy Scientific Press

*Corresponding author.
E-mail address: thakheru_a@cmu.ac.th (T. Akamine); teerapat.t@cmu.ac.th (T. Tosuai); romalramadhan29@gmail.com (R. Ramadhan); natthanan.p@cmu.ac.th (N. Promsuk); falan.s@chula.ac.th (F. Srisuriyachai); suparit.t@cmu.ac.th (S. Tangparitkul).

Received April 19, 2024; revised May 13, 2024; accepted June 4, 2024; available online June 10, 2024.

petroleum reservoirs between the two immiscible fluids of crude oil and aqueous phase is of interest in the current study-namely enhanced oil recovery (EOR).

With substantial oil ($> 40\%$) left unproduced in early stages of primary and/or secondary productions, EOR as tertiary production process is anticipated to improve microscopic oil displacement via optimizing fluid-fluid-rock interfacial phenomena and associated interactions (Deng et al., 2021). Different chemical agents (e.g., surfactants and alkali (Olajire, 2014; Bashir et al., 2022)) hence injected into target oil reservoir to manipulate or engineer such interfacial phenomena and interactions, with typical processes being a reduction in the oil-water interfacial tension and the oil-water-rock wettability alteration aimed to minimizing capillary resistance to the fluid displacement at pore-scale (Zhang et al., 2011; Singh et al., 2019). Recent studies further explored "engineered brine" (also known as low-salinity water or ion-tuned brine) and even nanofluids as potential displacing fluids in EOR process, although insights into EOR mechanisms contributed from these chemicals remain controversial (Agista et al., 2018; Katende and Sagala, 2019; Kazemzadeh et al., 2019; Olayiwola and Dejam, 2019).

For nanofluid EOR, background on colloid and interface science is crucial to elucidate its applicability to improve the oil displacement. Despite the fact that many studies reported nanofluid potential for EOR, great discrepancies in its mechanisms are observed. Interfacial activity of nanoparticles at the oil-water interface has been argued since solid nanoparticles (i.e., bare silica) could not energetically partition at the interface in the same manner as surfactants (Binks, 2002). Wettability modification to nanoparticle surface rather induces apparent interfacial partitioning and hence its consequent "apparent" reduction in the interfacial tension (Binks, 2002), of which more independent cross-investigations are needed to confirm such a controversy.

Nanoparticle-induced three-phase interaction at the triple-phase contact line is however a rather known process. This "three-phase" interaction refers to intricate interaction among solid substrate and immiscible fluids of oil and aqueous, which leads to the consequent wettability alteration (e.g., the three-phase contact angle). Nanoparticle self-arrangement at the water wedge constructs the oscillatory disjoining pressures that drive nanofilm to displace oil phase from solid substrate (Chengara et al., 2004; Wasan et al., 2011; Nikolov and Wasan, 2014), although such a mechanism has rarely been demonstrated and visualized in an immiscible displacement process. On such a "spreading nanofilm", the thin film theory was emphasized with additional structural disjoining pressure as contributed to the nanoparticle self-arrangement at the water wedge of the three-phase (Trokhymchuk et al., 2001). The structural disjoining pressure induced by the nanoparticles in aqueous solution develops the thin film thickness and the spreading dynamics as a function of time, whereas the spreading behavior is also a concentration-dependence as analytically demonstrated by Matar et al. (2007). Given the water film thickness exceeding the diameter of nanoparticles ($h \geq d$), the governing equation for the structural disjoining pressure (Π) expresses as (Tangparitkul et al., 2018; Nikolov et al., 2019):

$$\Pi = \Pi_0 \cos(\omega h + \phi_2) e^{-\kappa h} + \Pi_1 e^{-\delta(h-d)} \quad (1)$$

where d is the nanoparticle diameter, h is the water film thickness, and all other parameters (Π_0, Π_1, ω, ϕ_2, κ, and δ) are fitted as cubic polynomials varying with nanofluid concentration.

In addition, several studies considering influence of nanofluid concentration are limited to relatively high concentrations (1,000-50,000 ppm) (Hendraningrat et al., 2012; Maghzi et la., 2012; Cheraghian et al., 2017), where highly concentrated nanoparticles transportation in bulk fluid dominates fluid displacement and flow characteristics (such as log-jamming effect and nanoparticle aggregation (Hendraningrat et al., 2012; Bila et al., 2019)) and inevitably screens the effect of interfacial phenomena.

In the current study, the influence of nanoparticles on oil displacement process at pore-scale was examined using visualizable micromodel (i.e., optical lab-on-a-chip). Relatively low concentration nanofluids (≤ 500 ppm) were deliberately chosen to address the limited understanding of interfacial phenomena mentioned above. Studying at relatively lower concentrations is also relevant to oilfield applicability as injected nanofluids are inevitably diluted over traveling route from injection well to target reservoir, thus low-concentration mechanism of nanofluid EOR is crucial. Spatiotemporal oil displacement was qualitatively observed via a micromodel, while oil displacement efficiency was quantified to elucidate the nanofluid concentration dependency. The current research used the core-shell "polyvinylpyrrolidone-coated silica" nanoparticles owing to their capability to spontaneously partition at the oil-water interface without surfactant-like change to the interfacial energy (Tangparitkul and Yu, 2022). This allows pore-scale oil displacement process as an "independent cross-investigation" discussed above to be examined, without fluid-fluid interfacial energy to involve concurrently.

2. Materials and experimental methods

2.1 Chemicals and nanofluids

Throughout the study, two immiscible liquid phases are the oil and aqueous phase described hereafter. Aqueous phase may refer to either synthetic formation brine or nanofluids, as indicated.

Synthetic formation brine, mimicking that of Fang oilfields in Chiang Mai (Thailand), was made of 741 ppm sodium chloride (NaCl, 99.0%, RCI Labscan, Thailand) and 83 ppm calcium chloride ($CaCl_2 \cdot {}_2H_2O$, 99.0%, RCI Labscan, Thailand) salts dissolving in deionized water. The brine total dissolved solids are 824 ppm, which is equivalent to 13.42 mM in total.

Dead crude oil used in the current study collected from the same oilfields composes of high wax content of 51.0 wt% with slight asphaltenes of 0.05 wt% (Sukee et al., 2022). To only examine a capillary-dominated fluid displacement, inviscid oil was manipulated (without losing its surface-active species) by mixing the dead crude oil with toluene (RCI Labscan, Thailand) and heptane (99%, RCI Labscan, Thailand) at 1 : 1 : 1 ratio by mass at ambient condition. The mobility

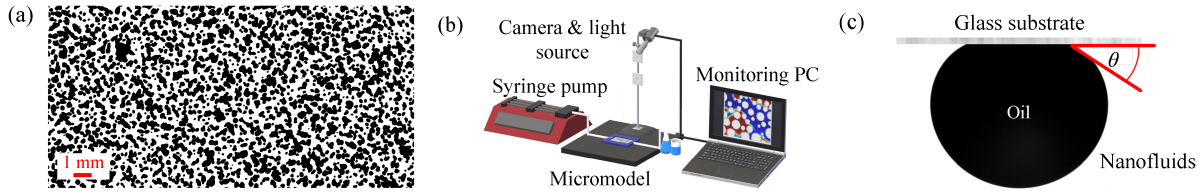

Fig. 1. (a) The micromodel pattern is reconstructed as reservoir rock network, with black areas indicating solid glass and white areas indicating pore-throat networks, shown with scale bar. (b) Schematics of experimental setup for oil displacement visualization consists of micromodel as porous medium, syringe pump for fluid injection, camera with light source for image acquisition, and monitoring computer. (c) The tree-phase contact angle is defined through the aqueous or nanofluid phase from image analysis.

ratio ($M = \mu_N/\mu_O$, where μ_N and μ_O are the viscosities of aqueous and oil phases, respectively) is calculated to be ~1.2, confirming a neglected viscous effect. The mixed oil (henceforth referred to as "the oil") has a density of 826.89 kg/m^3 and a viscosity of 1.11 mPa·s at 25 °C.

Nanofluids used in the study were specifically synthesized nanoparticles dispersed in deionized water at various concentrations. The nanoparticles are core-shell structure following the method conducted by Yu et al. (2017), which is briefly described as follows. The core nanoparticles are LUDOX® AS-40 colloidal silica (40 wt%, Sigma-Aldrich, USA), which is coated by polyvinylpyrrolidone (PVP, 40 kDa, Sigma-Aldrich, China) polymer. To prepare the PVP-coated silica nanoparticles, a 40 wt% silica nanoparticle suspension was initially diluted to 10 wt% and then introduced to Amberlite IRN 50 resin (Supelco®, USA) to eliminate excess SO_4^{2-} counterions. A 30 mL of the 10 wt% silica nanoparticle suspension was added dropwise to 40 mL of a 5 wt% of PVP solution under gentle stirring for 24 h, facilitating PVP adsorption onto the silica surface. Excess PVP was removed from the particle suspension through centrifugation for 4 h at 12,000 rpm. Compared to the silica core nanoparticles of ~9.2 nm in diameter, the PVP-coated nanoparticles have a larger hydrodynamic diameter of ~61.9 nm, with a polydispersity index of 0.25 measured by a Malvern ZetaSizer Nano ZS (Malvern Instrument, UK). Prior to each experiment, the nanofluids were freshly diluted to desired concentration and underwent a sonication for 15 min to ensure the nanoparticles being well-dispersed.

2.2 Micromodel set-up and oil displacement experiment

An as-received microfluidic chip (i.e., micromodel) made of transparent borosilicate glass in a pattern of physical rock network (Micronit B.V., The Netherlands) was used as a two-dimensional porous medium in the oil displacement experiment. The micromodel (20 mm × 10 mm × 0.02 mm thickness with average pore size of ~130 μm (Omran et al., 2020)) is designed to represent pore-throat structure of clastic reservoir rock, shown in Fig. 1(a). Porosity and permeability of the micromodel were measured to be ~50% with 2 μL of total pore volume and reported to be 2,620-2,940 mD (Pradhan et al., 2019), respectively.

The micromodel set-up is shown in Fig. 1(b), with main components being syringe pump, camera with light source, and monitoring computer. In the oil displacement experiment, the synthetic formation brine was initially injected to saturate the micromodel at 50 μL/min until complete brine saturation was attained (~ 1 min), before the injection rate was reduced to 0.1 μL/min and maintained for 1 h to allow residual fluids stabilized. The oil was thereafter injected to displace the residual brine at 50 μL/min until reaching the steady state (~1 min) before reduced to continuous injection at 0.1 μL/min for an overnight, where the initial oil saturation is defined (S_{Oi}). To initiate the oil displacement, the injection was switched to be the nanofluids at desired concentration at 0.1 μL/min until no more "displaced-oil" detected, taking ~ 3 pore volume injected (PVI), where the ultimate displacement efficiency (E_d) is determined (discussed below). The displacing injection rate of 0.1 μL/min was selected to ensure that the capillarity dominates the oil displacement (Laochamroonvorapongse et al., 2023), with calculated capillary number, $Ca = \mu_N v/(\sigma \cos\theta)$, of $\sim 6 \times 10^{-4}$, where v is the interstitial velocity (calculated to be 0.5 mm/min), θ the contact angle, and σ the interfacial tension. All displacement experiments were conducted at 25 °C temperature and ambient pressure.

To clean the micromodel after each use, a consecutive flooding process of four solvents (i.e., toluene, ethanol, deionized water, and 1 M NaOH solution, each at 50 μL/min injection rate) was performed to remove any residual substances and ensure pristine wettability of the solid surface. The solvent-cleaned micromodel was then physically cleaned by sonication and submerged in 1 M NaOH solution for 1 h, and another deionized water was injected to remove NaOH solution until effluence pH stabilized.

Throughout the oil displacement process, spatiotemporal fluid displacement in micromodel was acquisitioned using a digital microscopic camera (YiZhan, China) at 60 fps. The captured video was converted to be binary images using a Python programming to detect the solid micromodel with adaptive thresholding technique and separated two immiscible liquids by color, where the displaying images hereafter were designated the colors in blue, yellow, and black for aqueous, oil, and solid phases, respectively. A combination of Gaussian blur and image sharpening technique was also implemented to minimize noise effect (Safonov et al., 2008; Makandar and Halalli, 2015). The E_d was determined based on quantitative

Table 1. Nanofluid property and respective interfacial phenomena (μ_N, σ, and θ) and dimensionless numbers (M and Ca) with displacement performance at each nanofluid concentration.

Nanofluid concentration (ppm)	μ_N (mPa·s)	Interfacial phenomena		Dimensionless numbers		Displacement performance			
		σ (mN/m)	θ (°)	M	Ca	$\frac{\partial E_d}{\partial t}\|_i$ (%/PVI)	t_{BT} (PVI)	$E_d\|_{t_{BT}}$ (%)	E_d (%)
10	1.03	20.2	34.0	1.25	5.13×10^{-4}	54.0	0.61	32.3	52.3
50	1.03	16.5	32.3	1.25	6.14×10^{-4}	27.1	1.22	36.2	52.7
100	1.04	16.2	31.2	1.26	6.27×10^{-4}	24.2	1.62	34.9	36.8
500	1.05	15.6	11.3	1.27	5.72×10^{-4}	54.9	0.64	37.4	43.1

pixel counting, defined as $E_d = (P_{Oi} - P_O)/P_{Oi}$, where P_{Oi} and P_O are the numbers of pixels of the oil phase at the initial oil saturation and at a given time that the E_d calculated, respectively.

2.3 Measurements of the oil-aqueous interfacial tension and the three-phase contact angle

The oil-aqueous interfacial tension (σ) was measured by a pendent drop technique (Lee et al., 2008) using an Attension® Theta optical tensiometer (TF300-Basic, Biolin Scientific, Finland) operated at 25 °C, as per the oil displacement experiment conducted. The oil droplet of 15-20 μL was dispensed at the tip of a stainless inverted needle (gauge 22) surrounded by an aqueous phase, including nanofluids at different concentrations. The shape of the oil droplet was incubated and monitored at 3.3 fps until no detectable change was observed ($\sim$ 3 h). The σ was calculated using the Young-Laplace equation (Berry et al., 2015).

An "apparent" wettability of the oil-aqueous-glass system was characterized by the three-phase contact angle (θ) measured ex-situ using the same tensiometer and operated at the same condition to the σ measurement, though the glass slide (Hangzhou Rollmed, China) was used to represent the micromodel surface. An oil droplet of 10-15 μL was deposited underneath the glass slide by means of an inverted needle attached to a micro-syringe, and the contact angle was formed. The contact angle was recorded at 3.3 fps until the steady-state contact angle (no detectable change) was attained ($\sim$ 3 h). The contact angle was measured through the aqueous phase from image analysis using the OneAttention software, see Fig. 1(c). The average contact angle from the left and right is reported.

For both parameters, the measurements were conducted in triplicate and the average values were reported and used for further analyses. Detailed measurement approaches can be found in our previous works (Tangparitkul et al., 2018; Tangparitkul and Yu, 2022).

3. Results and discussion

3.1 Interfacial phenomena and characterization of dimensionless numbers

The measured σ and θ at elevated concentrations of nanofluids are reported in Table 1. With increasing nanofluid concentration, the "apparent" σ at the steady state ($\sim$ 3 h) were found to decrease slightly ($<$ 5 mN/m at the range of 10-500 ppm), with $\pm$0.5 mN/m experimental standard deviation observed. Reduction in the σ is a contribution of the nanoparticle partitioning at the oil-aqueous interface owing to the nanoparticle surface wettability functionalized, which is described as "apparent"-not energetically reduced-as previously observed (Tangparitkul and Yu, 2022). Such a slight concentration-dependent reduction in the σ has been emphasized by a continuing partitioning nature of nanoparticles at the liquid-liquid interface, approaching to a maximum of the nanoparticle interfacial coverage at the steady state of infinite time (Bizmark et al., 2014).

Even less concentration-dependency was observed in the measured θ at the experimented range of nanofluid concentration, the measured θ were roughly 30°-34°, with $\pm$6° experimental standard deviation. However, strong reduction in the θ was found (11.3°) at the highest concentration of 500 ppm, a reduction of $\sim$ 20°. This was likely due to the relatively high concentration (500 ppm) that was "high enough" to effectively construct additional structural forces between the oil-aqueous and aqueous-solid interfaces the structural disjoining pressure, although the measuring method by sessile drop could be not a direct indication for the structural disjoining pressure (Vafaei et al., 2006; Azarshin et al., 2017; Nikolov et al., 2019). All the measured θ are characterized the current three-phase system as strongly water-wet, albite arguably the "apparent" values.

To elucidate the oil displacement in the current study, two dimensionless numbers, namely M and Ca discussed above, were also determined and presented in Table 1. All resulted M are $\sim$ 1.2, confirming no viscous-dominated effect. The resulted Ca are much less than 1, echoing a capillary-dominated fluid displacement rather than that of viscous force. With such similar degrees of the dimensionless numbers obtained at all experimented concentrations, the oil displacement phenomena are not supposed to differ as contributed to the conventional interfacial phenomena owing to the nanofluid concentration per se, but rather other "unconventional" mechanisms.

3.2 Dynamic oil displacement and displacement efficiency

Given the aqueous phase (i.e., nanofluids) injected from the left-side to displace the residing oil toward the right-

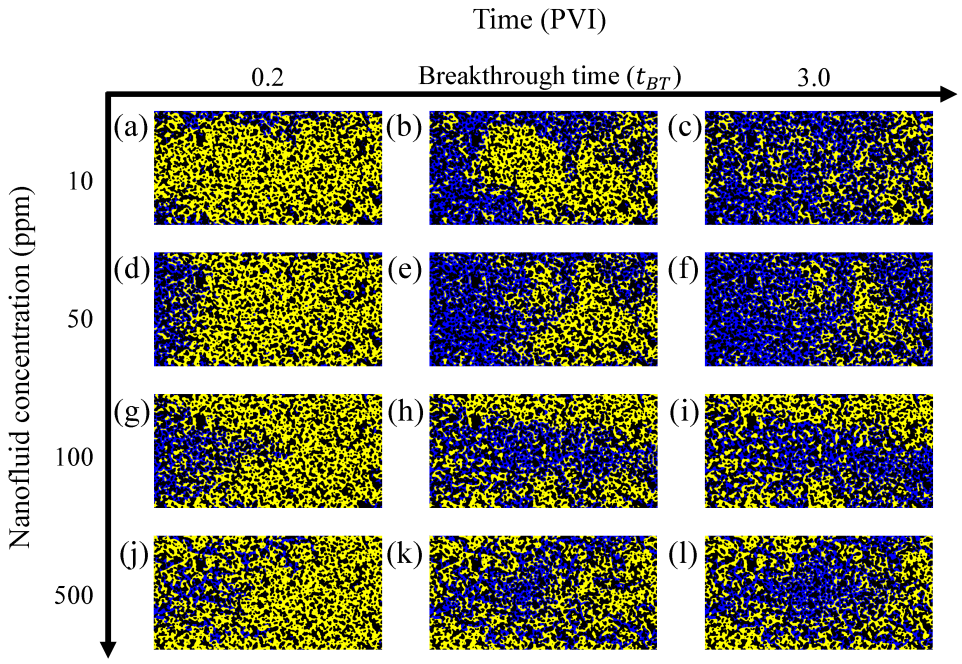

Fig. 2. Spatiotemporal development of oil displacement by nanofluids at (a)-(c) 10 ppm, (d)-(f) 50 ppm, (g)-(i) 100 ppm and (j)-(l) 500 ppm concentrations. Oil displacement results are shown at early stage of 0.2 PVI ((a), (d), (g) and (j)), the breakthrough time (t_{BT}; (b), (e), (h) and (k)), and steady-state 3.0 PVI time ((c), (f), (i) and (l)) for each concentration. Black, yellow, and blue areas indicate solid glass, displaced oil, and displacing nanofluid phases, respectively.

side effluence of the micromodel, Fig. 2 illustrates the spatial development of the oil displaced by the four nanofluids (10, 50, 100 and 500 ppm) at the three representing times. Initial stage of the displacement is shown at 0.2 PVI, while the later stage of the steady state where negligible changes in the oil displacement observed is taken at 3.0 PVI. The breakthrough time (t_{BT}) when the displacing nanofluid has reached the outlet effluence differs in each nanofluid concentration, as per reported in Table 1 and their respective images shown in Figs. 2(b), 2(e), 2(h) and 2(k), for 10, 50, 100 and 500 ppm, respectively, with arrows pointing shown in Fig. 3(a).

The oil displacement was quantitatively annotated as the dynamic E_d shown in Fig. 3(a), while the displacement efficiencies at the t_{BT} ($E_d|t_{BT}$) and at the steady state of $\sim$3.0 PVI (E_d) of each nanofluid concentration are compared in Fig. 3(b). The initial displacement rate $(\partial E_d/\partial t)|_i$ was also calculated (Table 1) to emphasize more on the dynamic displacement behavior.

At 10 ppm nanofluid concentration, a selective flow at the micromodel edges parallel to the displacement direction was observed at the initial period of displacement (Fig. 2(a)). This led to relatively early t_{BT} (0.6 PVI) and hence a small $E_d|t_{BT}$ of 32.5%, where the displacement adopted a fingering-like pattern (Fig. 2(b)). However, after the t_{BT} the oil displacement was developed for additional 19.8% and obtained the ultimate E_d of 52.3% at 3 PVI (Fig. 2(c)). Such an enhancement was attributed to consecutive pore-event of wetting layer flow (Blunt, 2017; Singh et al., 2017), of which the injected wetting aqueous phase wets the pore surface and cascades into wider area (both perpendicular and parallel to the displacement direction) and "swells" into pore-body space. The swelling of the aqueous phase elaborates to snap-off and/or cooperative pore filling events in the micromodel (Blunt, 2017; Singh et al., 2017), and inevitably leaves some of "un-displaced" or unconnected "trapped" oil ganglia behind-an obvious characteristics of a simple water wetting system (Payatakes, 1982), see Fig. 4.

Only discrepancy between 10 and 50 ppm concentrations were observed at the initial stage of the displacement dynamics ($t < t_{BT}$), while both quantitative and qualitative spaciotemporal displacement in the 50 ppm nanofluid were comparable to those of the 10 ppm after the t_{BT} (i.e., E_d is 52.7% at 3 PVI). Performance of the oil displacement in 50 ppm nanofluid, $(\partial E_d/\partial t)|_i = 27.1\%$/PVI and $t_{BT} = 0.61$ PVI, were slower than that of 10 ppm, $(\partial E_d/\partial t)|_i = 54.0\%$/PVI, where the oil displacement rather initially occurred at the micromodel edges and led to earlier breakthrough as discussed above. Faster $(\partial E_d/\partial t)|_i$ obtained in 10 ppm was likely a contribution from a higher σ (20.2 mN/m) that induced a stronger driving capillarity in the current water-wet system, compared to that of 50 ppm (16.5 mN/m) (Tangparitkul et al., 2023). Overall, the oil displacement performance behaved as that of the 10 ppm, with a fingering-like as the wetting layer swelled (Figs. 2(d)-2(f)). At the steady state (3.0 PVI), the trapped oil ganglia of which their areas are smaller than 50 μm^2 (average pore size $\sim$130 μm (Omran et al., 2020)) are of high amounts. Oil ganglia of 395 and 467 were counted at 3.0 PVI for the 10 ppm (Fig. 4(a)) and 50 ppm (Fig. 4(b)) nanofluids, respectively, although a cluster ($>$500 μm^2 area of the unconnected trapped oil) is spotted in both concentrations.

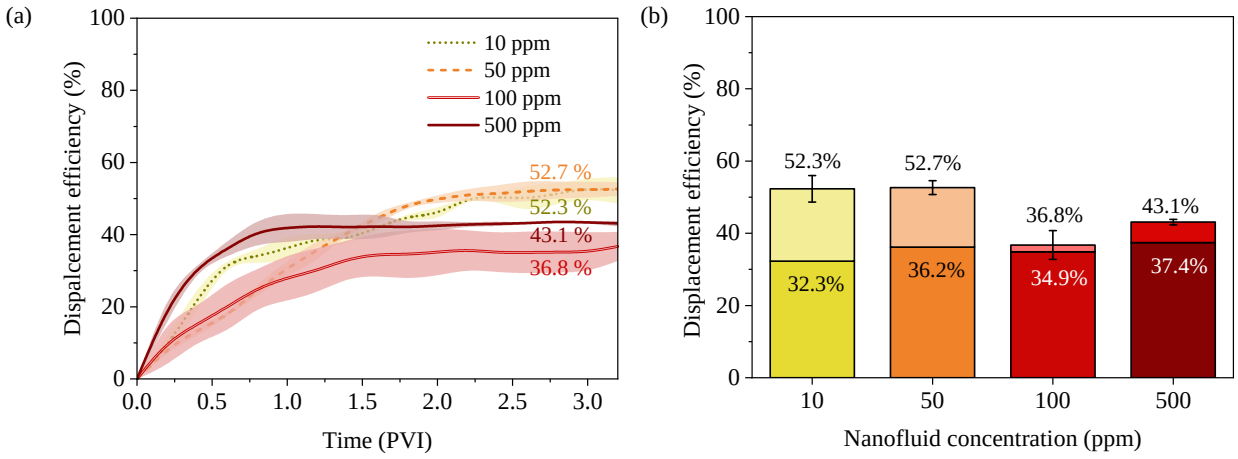

Fig. 3. (a) Oil displacement efficiency as a function of time for each nanofluid concentration, with inset arrows indicate the breakthrough time (t_{BT}) for each concentration. Shaded areas are experimental deviation and (b) displacement efficiencies at the t_{BT} (shown as darker color bars) and at the steady state ($\sim$ 3.0 PVI; shown as lighter color bars) are also annotated, with error bars being standard deviation.

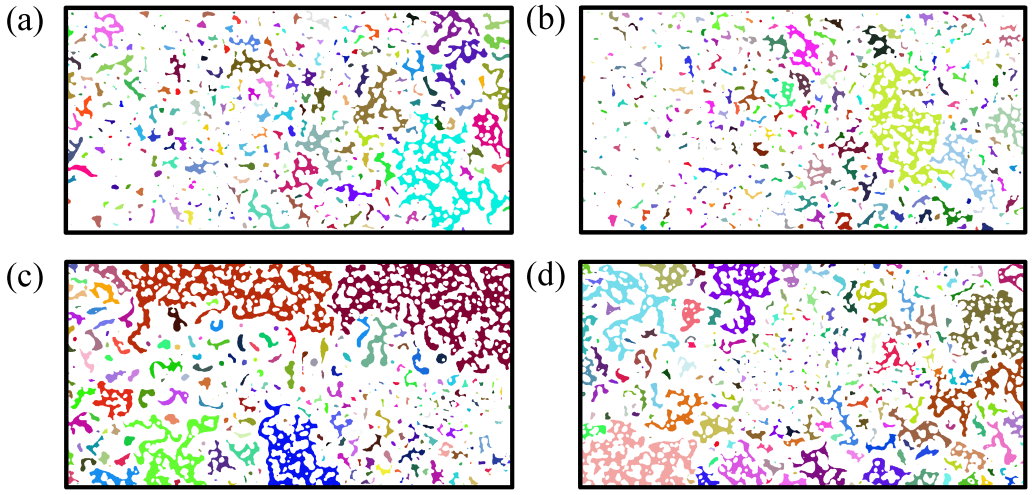

Fig. 4. Oil ganglia and clusters on micromodel at steady-state displacement (3.0 PVI) of (a) 10 ppm (a), (b) 50 ppm, (c) 100 ppm and (d) 500 ppm nanofluid concentrations. Non-connected ganglia and clusters are separated by different colors, while white areas refer to non-oil phase (i.e., solid glass and nanofluid phase combined).

At 100 ppm nanofluid concentration, the oil displacement was more populated into the middle of the micromodel rather than those of the edges as found in the lower concentrations, with distinct and large nanofluid intrusion in the center of the micromodel observed and a longer t_{BT} (1.62 PVI) obtained, see Figs. 2(g)-2(i). Such a lengthier initial displacement before the t_{BT} likely attributed to a sudden steady-state displacement, with relatively smaller additional oil displaced after the t_{BT} (1.9%, Fig. 3(b)). The swelling behavior in this 100 ppm nanofluid was found to be less apparent, compared to those previous two concentrations, with thinner nanofilm. Additionally, such an observation suggests a dependency of nanofluid concentration on the oil displacement behavior.

At 500 ppm nanofluid concentration, the oil displacement was attributed to high number of finger-like channels since the early state ($t < t_{BT}$, Fig. 2(j)), whereas the nanofluid film tended to "expand" or "swell-like" into the pore space. Such an "expanded part" subsequently led to enhanced oil displacement-likely a contribution from an increased nanofluid concentration, hence more additional oil was observed after the t_{BT} (5.7% increase at 3.0 PVI, Fig. 2(l)). Interestingly, it is worth to note that the displacement rate is of high $(\partial E_d/\partial t)|_i = 54.9\%$/PVI), likely also a contribution to high concentration.

Although a few un-displaced oil clusters (> 500 μm^2) were observed in the 100 and 500 ppm nanofluids (Figs. 4(c) and 4(d)), the smaller number of oil clusters were found in the 500 ppm (1 cluster) as likely attributed to an expanded part, compared to the no-expanded case of 100 ppm (with 2 clusters).

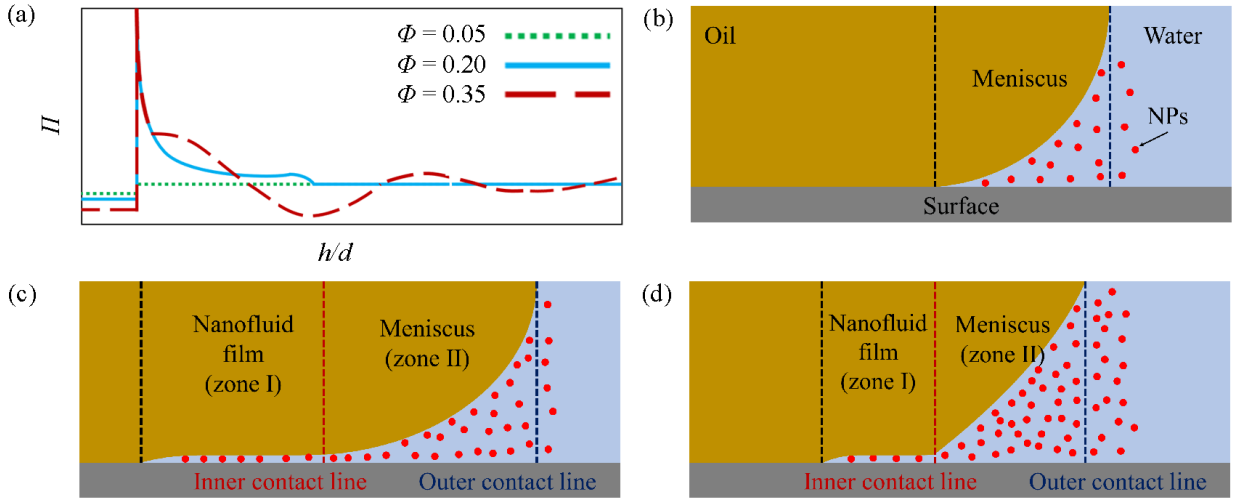

Fig. 5. (a) Analytical results on the structural disjoining pressure using Eq. (1) as a function of nanofluid concentration. Schematics of nanoparticle self-arrangement at the water wedge at elevated concentrations from: (b) No nanofluid spreading; to (c) nanofluid film spreading into inner contact line (Zone I) when the nanofluid concentration higher than the critical concentration; and to (d) nanofluid film spreading (Zone I) and meniscus expansion (Zone II) when the nanofluid concentration is relatively higher. Figures and plots are adapted from literature (Matar et al., 2007; Tangparitkul et al., 2018; Nikolov et al., 2019).

3.3 Oil displacement mechanisms at pore-scale

Considering the water-wet system, two pore-scale mechanisms were found in the oil displacement investigated in the current study. The first mechanism is the wetting layer flow and the subsequent the wetting film swelling (Blunt, 2017; Singh et al., 2017), which was primarily observed at 10 ppm and 50 ppm nanofluids. The second is the nanofluid spreading as attributed to the structural disjoining pressure (Tangparitkul et al., 2018; Nikolov et al., 2019), which is thought to dominate at 100 ppm and 500 ppm nanofluids.

For the wetting layer flow, wetting fluid (as the aqueous phase in the current study) has a strong affinity to surface of porous medium, and leads to its preference to wet and cascade to flow along the surface edges. As a result of such a continuing flow, the wetting layer further swells as a wetting film into the pore-body space and hence displaces the non-wetting phase (Tørå et al., 2012; Blunt, 2017; Singh et al., 2017).

Based on Eq. (1), the nanofluid concentration governs the magnitude of structural disjoining pressure (Π) via the fitting parameters, and thus leads to report on critical nanofluid concentration of 0.30 volume fraction (ϕ) in order to acquire an effective magnitude of Π constructed (Chu et al., 1994; Manne and Warr, 1999). Fig. 5(a) exemplifies nanofluid-induced Π magnitude as a function of concentration, where the ϕ of 0.35 (greater than the critical ϕ of 0.30) constructs a stronger repulsive oscillatory disjoining pressure, and hence initiates a nanofluid spreading (Matar et al., 2007). Lower nanofluid concentrations (lower than the critical ϕ) do not facilitate such addition repulsive forces.

Schematics of the nanoparticle accumulation in the water wedge at the triple-phase contact line illustrate various interfacial behaviors at elevated nanofluid concentrations, shown in Figs. 5(b)-5(d). Relatively low concentration induces no nanofluid spreading (Fig. 5(b)), while the interface meniscus controls the contact line. Due to a strong Π at higher than critical concentration, the nanofluid film spreading into inner contact line (Zone I), see Fig. 5(c). With relatively higher concentration, nanofilm spreads (Zone I) and the meniscus further expands (Zone II), see Fig. 5(d).

With the observed results from 10 and 50 ppm nanofluids, development of the wetting layer flow is obvious throughout the micromodel as annotated by the 2.25 mm^2 area of displacement shown in Fig. 6. Within just 60 s time period, the wetting layer flow swelled to thicker film and led to a "snap-off" event (Blunt, 2017; Singh et al., 2017), see Figs. 6(a)-6(c) and Figs. 6(d)-6(f). The thicker wetting film develops at the narrower throats (arrows pointed in Figs. 6(a), 6(b), and 6(e)) induced the non-wetting phase of oil collapsed or pinched off, which left oil ganglia entrapment (circles in Figs. 6(b), 6(c), and 6(f)). Such pore-scale mechanisms have been widely reported in a typical water-wet system (Zhao et al., 2016; Singh et al., 2017; Primkulov et al., 2021), suggesting that nanoparticles do not likely contribute to the oil displacement per se at these low concentrations. No significant change in the measured θ (Table 1) at these concentrations also confirm negligible nanoparticle direct contribution to the oil displacement.

At higher nanofluid concentrations of 100 and 500 ppm, the nanoparticle interaction becomes effective and nanofluid spreading dominates the oil displacement. Applying the theory of nanoparticle structural force for the 500 ppm, $\Pi = 2\sigma\cos(\pi/2-\theta)/r$ (Nikolov and Wasan, 2014), the Π of the nanofilm between the crude oil and solid surface is 0.71 Pa. With the Eq. (1) and assuming ϕ of 0.30, the incipient film thickness is $\sim$ 80.5 nm, which can thus accommodate the

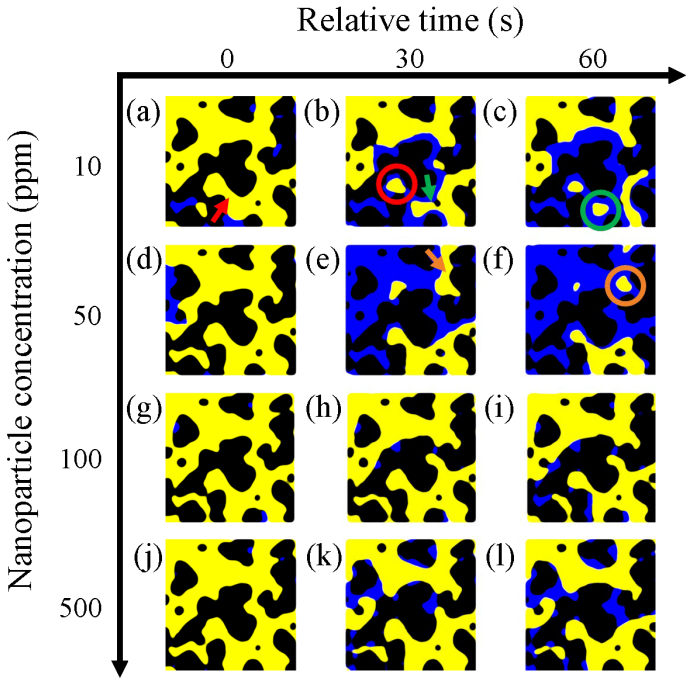

Fig. 6. Pore-scale displacement of 2.25 mm^2 area at (a)-(c) 10 ppm, (d)-(f) 50 ppm, (g)-(i) 100 ppm and (j)-(l) 500 ppm nanofluids, comparing pore-scale events developing over same period of time (60 s). Pairs of same-colored arrow and circle indicate where snap-off events occurred: Red and green are of 10 ppm nanofluid while orange is of 50 ppm nanofluid. Snap-off events did not likely occur in 100 and 500 ppm nanofluids. Black, yellow, and blue areas indicate solid glass, displaced oil, and displacing nanofluid phases, respectively.

$\sim$ 61.9 nm nanoparticles. As opposed to those lower concentrations, the pore-scale displacement in the 100 and 500 ppm hardly found snap-off event, e.g., Figs. 6(g)-6(l), reflecting a different mechanism. With increasing nanofluid concentration, more effective structural disjoining pressure potentially leads to more stable nanofilm and stronger spreading (Zone I in Figs. 5(c) and 5(d). Such a behavior was observed in the current study, whereas the oil displacement was accelerated at higher nanofluid concentration. The $(\partial E_d/\partial t)|_i$ increased from 24.2%/PVI at 100 ppm to 54.9%/PVI at 500 ppm, while the t_{BT} was shorter for 500 ppm (1.62 PVI $\rightarrow$ 0.64 PVI)-achieving a greater oil displacement. The nanofluid meniscus expansion (Zone II in Fig. 5(d)) was also observed in 500 ppm (Figs. 6(k) and 6(l)), which led to additional oil displaced after the t_{BT}.

4. Conclusions

Specially synthesized core-shell nanoparticles-with no energetically interfacial responsiveness-have been used to elucidate the contribution of nanofluid concentration to oil displacement process at pore-scale using micromodel visualization technique. Relatively low concentrations (10-500 ppm) of nanofluids were examined on the crude oil displacement dynamics, while the spaciotemporal performance was characterized quantitatively and qualitatively via image processing technique. Based on the experimental results above, the study can be concluded as follows:

1) At the experimented concentrations, a reduction in the ex-situ three-phase oil-aqueous-glass contact angle was found at the highest concentration of 500 ppm-a contribution from the nanoparticle-induced structural disjoining pressure. Although a significant reduction in the crude oil-nanofluid interfacial tension cannot be concluded as same as the consequent displacement performance at the steady-state, dynamics performance of crude oil displacement likely associated with such a reduction in the interfacial tension and therefore further research is needed for full understanding.
2) At the low nanofluid concentrations (10 and 50 ppm), the wetting layer flow dominated the oil displacement of which the wetting layer swelled into pore space and led to snap-off events, more evidently at narrow throats. As a consequence, the non-wetting oil phase collapsed and pinched off, leaving a high amount of small oil ganglia trapped in confined pore-space. Such a displacement behavior is a nature of strongly wetting phase that invades into porous medium, stressing that no contribution from nanoparticles can be justified to the displacement process at these concentrations.
3) Nanofluid concentration is at play at higher concentrations (100 and 500 ppm), the nanoparticle self-arrangement at the water wedge induced the structural disjoining forces between the oil-aqueous and solid-aqueous interfaces leading to nanofluid spreading, which was further improved at higher concentration.

The nanofluid spreading controlled the oil displacement spaciotemporal performance, with snap-off events hardly observed. At higher 500 ppm nanofluid, more stable nanofilm and stronger spreading developed as a result of meniscus expansion, resulting in faster displacing dynamics and additional oil displaced after the breakthrough time.

The current study thoroughly addresses the influence of the nanoparticle concentration on the crude oil displacement at pore-scale, with the aim for better design the immiscible fluid displacement process, such as enhanced oil recovery and CO_2 geological storage applications. Relatively low concentrations examined, which are not widely explored, revealed some significant nanoparticle interfacial behaviors associated with pore-scale fluid flow and displacement, of which should be served as fundamental to further investigation and future research.

Acknowledgements

Financial support for this work is greatly acknowledged with contributions from Office of the Permanent Secretary for Ministry of Higher Education, Science, Research and Innovation (No. RGNS 64-081) (S. Tangparitkul); Thailand Science Research and Innovation (TSRI) (S. Tangparitkul); Thailand Toray Science Foundation (TTSF 2022-16) (S. Tangparitkul); and Faculty of Engineering, Chiang Mai University (S. Tangparitkul and T. Akamine). The authors would like to thank Dr. Artorn Anuduang (Universiti Kebangsaan Malaysia, Malaysia) for helping with sample centrifugation.

Conflict of interest

The authors declare no competing interest.

References

Agista, M. N., Guo, K.,Yu, Z. A state-of-the-art review of nanoparticles application in petroleum with a focus on enhanced oil recovery. Applied Sciences, 2018, 8(6): 871.

Azarshin, S., Moghadasi, J., A Aboosadi, Z. Surface functionalization of silica nanoparticles to improve the performance of water flooding in oil wet reservoirs. Energy Exploration & Exploitation, 2017, 35(6): 685-697.

Bashir, A., Haddad, A. S., Rafati, R. A review of fluid displacement mechanisms in surfactant-based chemical enhanced oil recovery processes: Analyses of key influencing factors. Petroleum Science, 2022, 19(3): 1211-1235.

Berry, J. D., Neeson, M. J., Dagastine, R. R., et al. Measurement of surface and interfacial tension using pendant drop tensiometry. Journal of Colloid and Interface Science, 2015, 454: 226-237.

Bila, A., Stensen, J. Å.,Torsæter, O. Experimental evaluation of oil recovery mechanisms using a variety of surface-modified silica nanoparticles in the injection water. Paper SPE 195638 Presented at the SPE Norway One Day Seminar, Bergen, Norway, 14 May, 2019.

Binks, B. P. Particles as surfactants-similarities and differences. Current Opinion in Colloid & Interface Science, 2002, 7(1-2): 21-41.

Bizmark, N., Ioannidis, M. A.,Henneke, D. E. Irreversible adsorption-driven assembly of nanoparticles at fluid interfaces revealed by a dynamic surface tension probe. Langmuir, 2014, 30(3): 710-717.

Blunt, M. J. Multiphase Flow in Permeable Media: A Pore-Scale Perspective. London, UK, Cambridge University Press, 2017.

Chengara, A., Nikolov, A. D., Wasan, D. T., et al. Spreading of nanofluids driven by the structural disjoining pressure gradient. Journal of Colloid and Interface Science, 2004, 280(1): 192-201.

Cheraghian, G., Kiani, S., Nassar, N. N., et al. Silica nanoparticle enhancement in the efficiency of surfactant flooding of heavy oil in a glass micromodel. Industrial & Engineering Chemistry Research, 2017, 56(30): 8528-8534.

Chu, X., Nikolov, A., Wasan, D. Monte Carlo simulation of inlayer structure formation in thin liquid films. Langmuir, 1994, 10(12): 4403-4408.

Deng, X., Tariq, Z., Murtaza, M., et al. Relative contribution of wettability Alteration and interfacial tension reduction in EOR: A critical review. Journal of Molecular Liquids, 2021, 325: 115175.

Hendraningrat, L., Shidong, L., Torsœter, O. A glass micromodel experimental study of hydrophilic nanoparticles retention for EOR project. Paper SPE 159161 Presented at the SPE Russian Oil and Gas Exploration and Production Technical Conference and Exhibition, Moscow, Russia, 16-18 October, 2012.

Katende, A., Sagala, F. A critical review of low salinity water flooding: Mechanism, laboratory and field application. Journal of Molecular Liquids, 2019, 278: 627-649.

Kazemzadeh, Y., Shojaei, S., Riazi, M., et al. Review on application of nanoparticles for EOR purposes: A critical review of the opportunities and challenges. Chinese Journal of Chemical Engineering, 2019, 27(2): 237-246.

Laochamroonvorapongse, R., Beunat, V., Pannacci, N., et al. Direct investigation of oil recovery mechanism by polymer-alternating-Gas CO_2 through micromodel experiments. Energy & Fuels, 2023, 37(20): 15603-15614.

Lee, B. B., Ravindra, P., Chan, E. S. A critical review: surface and interfacial tension measurement by the drop weight method. Chemical Engineering Communications, 2008, 195(8): 889-924.

Maghzi, A., Mohammadi, S., Ghazanfari, M. H., et al. Monitoring wettability alteration by silica nanoparticles during water flooding to heavy oils in five-spot systems: A pore-level investigation. Experimental Thermal and Fluid Science, 2012, 40: 168-176.

Makandar, A., Halalli, B. Image enhancement techniques using highpass and lowpass filters. International Journal of Computer Applications, 2015, 109(14): 12-15.

Manne, S., Warr, G. Supramolecular structure of surfactants confined to interfaces, in Supramolecular Structure in

Confined Geometries, edited by Manne, S. and Warr, G., ACS Symposium Series, Washington, pp. 2-23, 1999.

Matar, O., Craster, R., Sefiane, K. Dynamic spreading of droplets containing nanoparticles. Physical Review E, 2007, 76(5): 056315.

Nikolov, A., Wasan, D. Wetting–dewetting films: The role of structural forces. Advances in Colloid and Interface Science, 2014, 206: 207-221.

Nikolov, A., Wu, P., Wasan, D. Structure and stability of nanofluid films wetting solids: An overview. Advances in Colloid and Interface Science, 2019, 264: 1-10.

Olajire, A. A. Review of ASP EOR (alkaline surfactant polymer enhanced oil recovery) technology in the petroleum industry: Prospects and challenges. Energy, 2014, 77: 963-982.

Olayiwola, S. O., Dejam, M. A comprehensive review on interaction of nanoparticles with low salinity water and surfactant for enhanced oil recovery in sandstone and carbonate reservoirs. Fuel, 2019, 241: 1045-1057.

Omran, M., Akarri, S., Torsaeter, O. The effect of wettability and flow rate on oil displacement using polymer-coated silica nanoparticles: A microfluidic study. Processes, 2020, 8(8): 991.

Payatakes, A. Dynamics of oil ganglia during immiscible displacement in water-wet porous media. Annual Review of Fluid Mechanics, 1982, 14(1): 365-393.

Pradhan, S., Shaik, I., Lagraauw, R., et al. A semi-experimental procedure for the estimation of permeability of microfluidic pore network. MethodsX, 2019, 6: 704-713.

Primkulov, B. K., Pahlavan, A. A., Fu, X., et al. Wettability and Lenormand's diagram. Journal of Fluid Mechanics, 2021, 923: A34.

Safonov, I. V., Rychagov, M. N., Kang, K., et al. Color Imaging XIII: Processing, Hardcopy, and Applications, Adaptive sharpening, edited by Safonov, I. V., SPIE, California, pp. 256-267, 2008.

Singh, K., Jung, M., Brinkmann, M., et al. Capillary-dominated fluid displacement in porous media. Annual Review of Fluid Mechanics, 2019, 51: 429-449.

Singh, K., Menke, H., Andrew, M., et al. Dynamics of snap-off and pore-filling events during two-phase fluid flow in permeable media. Scientific Reports, 2017, 7(1): 5192.

Sukee, A., Nunta, T., Haruna, M. A., et al. Influence of sequential changes in the crude oil-water interfacial tension on spontaneous imbibition in oil-wet sandstone. Journal of Petroleum Science and Engineering, 2022, 210: 110032.

Tangparitkul, S., Charpentier, T. V., Pradilla, D., et al. Interfacial and colloidal forces governing oil droplet displacement: Implications for enhanced oil recovery. Colloids and Interfaces, 2018, 2(3): 30.

Tangparitkul, S., Sukee, A., Jiang, J., et al. Role of interfacial tension on wettability-controlled fluid displacement in porous rock: A capillary-dominated flow and how to control it. Capillarity, 2023, 9(3): 55-64.

Tangparitkul, S., Yu, K. Crude oil-water interface partitioning of polyvinylpyrrolidone-coated silica nanoparticles in low-salinity brine. Journal of Petroleum Science and Engineering, 2022, 211: 110185.

Tørå, G., Øren, P. E., Hansen, A. A dynamic network model for two-phase flow in porous media. Transport in Porous Media, 2012, 92: 145-164.

Trokhymchuk, A., Henderson, D., Nikolov, A., et al. A simple calculation of structural and depletion forces for fluids/suspensions confined in a film. Langmuir, 2001, 17(16): 4940-4947.

Vafaei, S., Borca-Tasciuc, T., Podowski, M., et al. Effect of nanoparticles on sessile droplet contact angle. Nanotechnology, 2006, 17(10): 2523.

Wasan, D., Nikolov, A., Kondiparty, K. The wetting and spreading of nanofluids on solids: Role of the structural disjoining pressure. Current Opinion in Colloid & Interface Science, 2011, 16(4): 344-349.

Yu, K., Zhang, H., Hodges, C., et al. Foaming behavior of polymer-coated colloids: The need for thick liquid films. Langmuir, 2017, 33(26): 6528-6539.

Zhang, C., Oostrom, M., Wietsma, T. W., et al. Influence of viscous and capillary forces on immiscible fluid displacement: Pore-scale experimental study in a water-wet micromodel demonstrating viscous and capillary fingering. Energy & Fuels, 2011, 25(8): 3493-3505.

Zhao, B., MacMinn, C. W., Juanes, R. Wettability control on multiphase flow in patterned microfluidics. Proceedings of the National Academy of Sciences, 2016, 113(37): 10251-10256.